Continuous direct current by charge transportation for next-generation IoT and real-time virtual reality applications

Jianxiong Zhu [a,b,c,1], Hao Wang [a,b,c,d,1], Zixuan Zhang [a,b,c,1], Zhihao Ren [a,b,c],
Qiongfeng Shi [a,b,c], Weixin Liu [a,b,c], Chengkuo Lee [a,b,c,e,*]

a Department of Electrical and Computer Engineering, National University of Singapore, Singapore
b Center for Intelligent Sensors and MEMS (CISM), National University of Singapore, Singapore
c NUS Suzhou Research Institute (NUSRI), Suzhou, China
d Institute of Biomedical & Health Engineering, Shenzhen Institutes of Advanced Technology (SIAT), Chinese Academy of Sciences (CAS), Shenzhen, 518035, China
e NUS Graduate School for Integrative Science and Engineering (NGS), National University of Singapore, Singapore

ARTICLE INFO

ABSTRACT

A conversion from mechanical energy into direct current (DC) is of great interest to realize the next-generation self-sustained Internet of Things (IoT) and real-time virtual reality (VR) control. Inspired by ancient waterwheel transport water and P–N junction theory, a continuous DC nanogenerator was developed using charges unidirectional transportation and dual-intersection triboelectric nanogenerators (TENGs). By employing tribo-polarity reversal porous material as charges transportation carrier sliding among the ultra-negative and ultra-positive materials, the charges were unidirectionally transported by the discharge of repulsion via line electrodes, forming a stability DC output. Due to the charge transport and repulsive discharge, a much higher DC output voltage was easily obtained than the air breakdown mechanism. Moving forward the realistic application, the capability of the dual-intersection TENGs as a DC power source for the actuator and sensor was well demonstrated, and it further expanded all kinds of wireless networks for next-generation IoT to directly power sensor nodes. To get across the discontinuous characteristic identification from triboelectric (e.g. frequency, number of peaks, pulse absolute value) as status stimulation in software, we first time successfully realized a continuous motion control in virtual space for next-generation real-time VR application in triboelectric.

1. Introduction

As a fast technology development of the fifth-generation cellular network technology (5G), everything is connecting in a much easier way by the Internet of Things (IoT) [1–4] and virtual reality (VR). In a typical IoT framework, the battery-charged solution enables remote ubiquitous sensor nodes could be low cost and massively deployed. Therefore, direct current (DC) plays an increasingly important role in the realization of such IoT sensor networks and VR scenarios, where electronic devices provide an extremely convenience for human beings living qualities [5–12]. To solve the energy crisis issue and achieve sustainable environment-friendly development, intensive works by researchers have been dedicated to converting environmental mechanical energy into electricity to meet the demand for a clean and sustainable power source [13–16]. However, almost all the vibration-based power generators in renewable energy are producing the alternating current (AC), which is inconvenient for direct use in the IoT and linear motion control in VR applications. While the IoT sensor nodes are still relying on battery-based DC power source, the associated issue of using battery including potential environmental contamination and required labor of battery exchange, etc. All those issues become the drawbacks to be resolved. Besides, the DC output without any extra electronic units gives a straightforward and energy-efficient design of control interface for further VR scenario applications.

Triboelectric nanogenerator (TENG) was first proposed in 2012 [17–19,76–80], and it has been demonstrated as a cost-effective, clean, and sustainable strategy to convert mechanical energy into electricity with its comprehensive advantages including small size and a wide choice of materials [20–28,81–85]. By leveraging the tribo-electrification effect and electrostatic induction in two dissimilar

materials with opposite tribo-polarity, the TENG enables a simple but effective mechanical-to-electrical energy conversion by contact-separation or sliding with a wide range of material selection [29, 30]. To reach a DC output from TENG, TENG needs a combination of a bridge rectifier (AC-DC transformation) [31–36] and auxiliary management electronic units to obtain a stable DC output [37–40], which takes away its portability advantage and its energy usage efficiency due to extra power consumption. Many attempts to achieve charge directionally flow for direct DC output using 2D material [41] or a unique mechanical structure [42–44] in TENG. However, those trials "DC" output from their nanogenerators came from a step charge increasing (Inappropriate to directly claim DC output) or presented in a low output voltage (maximum 1.37 V) due to the air breakdown in conventional TENG [43]. On the other hand, the triboelectric materials (lose electrons or obtain electrons during their friction) in the energy harvesting were widely investigated recently [19,45–59]. However, no group yet has carried out the research regarding multi-materials for charges unidirectional flow, such as using ultra-positive (easily lose electrons),

ultra-negative (easily obtain electrons), and tribo-polarity reversal porous material.

To reach a DC output for a directly powering versatile electronic elements in typical IoT framework and further its application [60–70, 86–90] in real-time VR motion control, inspired by ancient waterwheel to transport water from a low site to a relatively high location by mechanic power for stable water flow and P–N junction theory. By leveraging off the rotation-structure [20,71,72] TENG in a direction sliding, to get across conventional AC output, we proposed a novel mechanism continuous DC dual intersection TENGs (DC-DTENG). The charges generated by friction was transported by a tribo-polarity reversal porous material from a low potential to a high potential, and then it was released by the discharge of repulsion with easily ~5 times higher output voltage than the conventional TENG. Moving forward the practical application, the performance of the DC-DTENG was demonstrated by a soft switch, an ultraviolet (UV) radiation sensing and a wireless module with a smartphone for next-generation IoT to directly power sensor nodes. Furthermore, to overcome the discontinuous
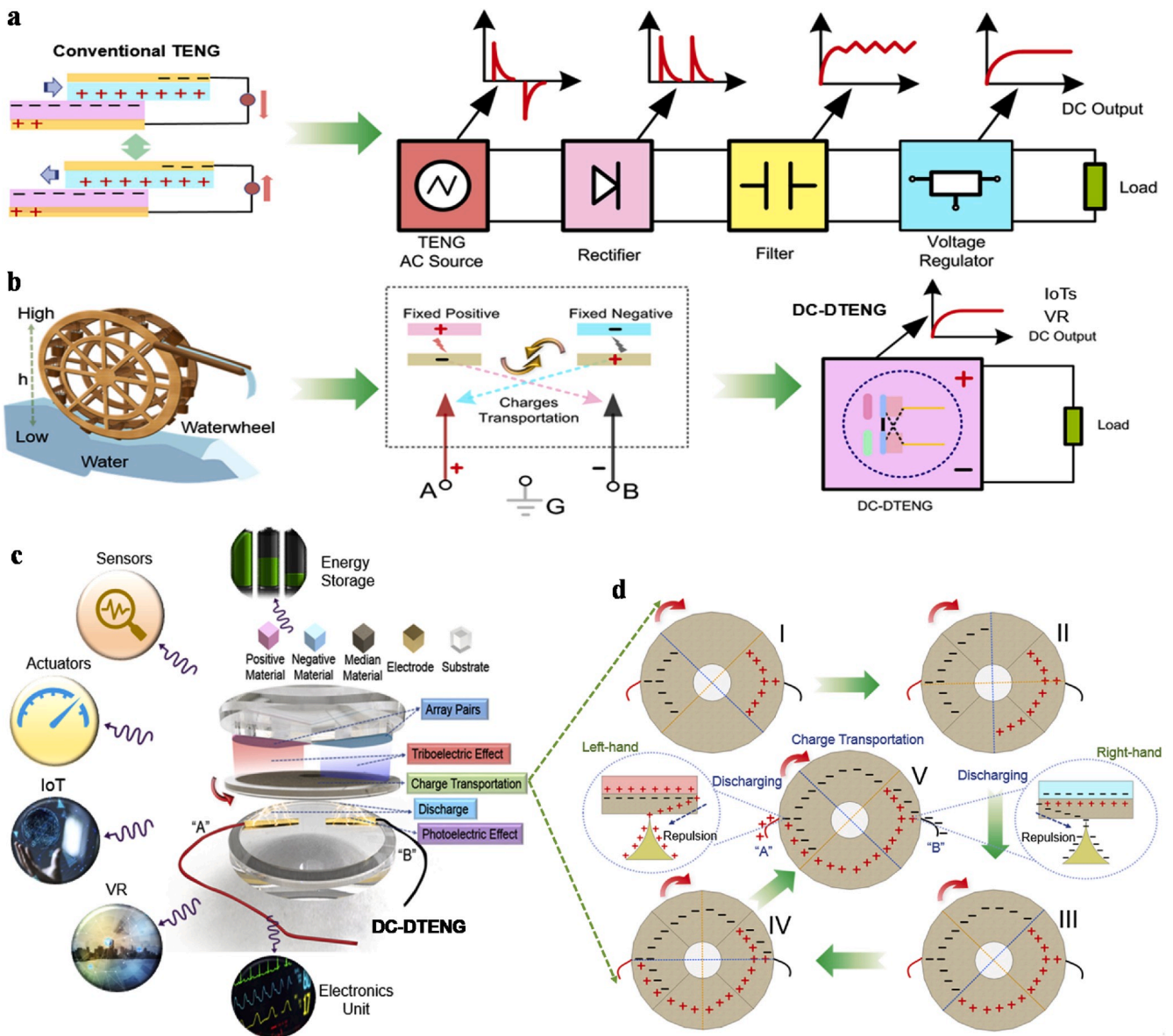
Fig. 1. Schematic illustration and working principle of DC-DTENG. (a) Conventional triboelectric generator using external electric units for DC output, and (b) inspired by a waterwheel system, a continuous DC output with an all-structure design. (c) Schematic diagram of DC-DTENG and its various applications. (d) The working process of the DC-DTENG during a period in charge generation, charges transportation, and charges releasing by repulsive force.

characteristic information identification (e.g. frequency, number of peaks or absolute value range is always defined as a status stimulation in software) in the triboelectric, we the first time successfully realized continuous motion control in virtual space for the next-generation real-time VR scenario applications.

2. Results and discussion

2.1. Design and working mechanism of DC-DTENG

To obtain DC from conventional TENG or vibration-based power source, a combination of a bridge rectifier (AC-DC transformation) and auxiliary management electronic are needed as shown in Fig. 1a. However, the extra electronic elements with their power consumption would decrease their energy usage efficiency. Waterwheel with ancient wisdom was created for water transportation from a low site to a comparatively high location. Inspired by the water transportation phenomenon from a waterwheel and the idea from Van De Graaff generator [73–75] with a belt as a transportation carrier, a continuous DC output with in-plane structure was produced by a similar mechanism from a low voltage potential to a comparative high potential as shown in Fig. 1b and Fig. S1 Supplementary Information. To achieve a unidirectional current flow for a continuous DC output, a TENG mechanism of dual intersection power sources was proposed, involving charges transportation by the carrier and its repulsive discharge to electrodes. Moreover, the advantage of this mechanism provides a practical solution to obtain the mechanical activity information which is directly related to the output signal (almost not any information loss due to without any extra electronic units) It was observed a straightforward and energy-efficient design of control interface for further scenario applications. Here, tribo-polarity reversal porous material (sliding layer) as charges transportation carrier was sliding among the ultra-negative and ultra-positive dielectric materials (fixed layer), generating triboelectric charges on the disk-carrier and fixed layers. By rotating the sliding layer, the charges on the carrier were continuously unidirectional transported from a location (a fixed layer left-hand, low potential) to another (fixed layer right-hand, high potential), and it easily discharged to electrodes by the repulsive force due to the same triboelectric charges on the fixed layer behind. Finally, the repulsive force released the transportation charges to the closest electrode in a continuous DC output. Based on this mechanism, a simplified prototype was designed as shown in Fig. 1c, which contained a rotator and two stators with a sandwich structure. With the DC output from the DC-DTENG, it depicts a potential wide range of applications, such as for actuator, an ultraviolet (UV) radiation sensing, energy storage, and a wireless module with a smartphone for IoT, and real-time control for next-generation VR. To further investigate its mechanism, the charges and potential simulation by the finite element analysis (FEA) in COMSOL software were carried out in Fig. S2. It observed that the output current, referring to the charge generation, transportation and discharging, was determined by rotational speeds of a disk.

The detail working mechanism of the DC-DTENG is shown in Fig. 1d. Initially, no charges were on the disk. As the clockwise rotation starts, the friction between the disk and the fixed layer generated both positive (right-hand quarter) and negative (left-hand quarter) charges on the disk itself as shown in Fig. 1d(I). It was noted that a quarter area of ultra-positive material was located on the left-hand above disk with a pink color, whereas the right-hand ultra-negative material was with a light blue. Fig. 1d(II to III) depicted that the disk motioned clockwise until 90°. The charges on the left-hand of the disk transported along with carrier itself, and the more charges on the left-hand quarter generated on the surface of the disk due to the triboelectric effect. It was the same to the right-hand quarter but with opposite charges due to the ultra-negative material versus (vs) disk. The disk here presents positive surface charges when it is friction against ultra-negative material, and it appears negative surface charges when it contacts an ultra-positive

material. As the disk goes further in Fig. 1d(IV), the charges on the disk arrived at the position of another fixed layer carrying the charges with the same polarity. Therefore, the transportation charges along with the disk-carrier were repelled by the charges on the fixed layer and were discharged to an electrode which was very close to the disk. Due to the three different tribo-polarity materials in order and the charges transportation, the charges on the disk would repel away by the same charges, instead of neutralization. Coupling with triboelectric effect, the tribo-polarity reversal porous material facing against an ultra-positive and an ultra-negative material, charges transportation mechanism along with a disk, and electron pair repulsion theory, the continuous DC output produced from two electrodes. Finally, the continuous rotation of the disk formed a stable continuous DC output as shown in Fig. 1d(V). Theoretically, the DC-DTENG could generate more power than conventional TENG due to the continuous charge transportation and discharges, which would dramatically save the rest time (Conventional TENG) during the operation.

2.2. Tribo-polarity reversal porous material and its wave curve regulation

The "median material" is defined as a material among an ultra-positive material and ultra-negative material as shown in Fig. 2a. The logic of this selected "median material" is a tradeoff of triboelectric electrons in losing or obtaining. For example, the "median material" porous cloth (Polyester) presents positive surface charges when it is friction against ultra-negative material (PVC, polyvinyl chloride), and it appears negative surface charges when it contacts an ultra-positive material (PMMA, Poly(methyl methacrylate)) as shown in Fig. 2b. It notes that plenty of materials could be as median materials with the logic of three tribo-polarity materials in order, such as natural rubber, paper, etc. Fig. S3 was a systematic measurement for the chosen ultra-positive material and the ultra-negative material in our experiments. Facing against the PVC and PMMA, it found that the tribo-polarity reversal porous cloth was as an ideal "median material" due to its mechanic robust and flexibility as a friction layer. The "median material" porous material was measured as shown in Fig. S4 to demonstrate the triboelectric electrical performance with different contact areas. It concluded that with a larger contact area, a higher V_{oc} and more transferred charges were obtained. To further investigate the electrical property of the tribo-polarity reversal porous cloth between the PMMA and PVC, the transferred charges and open-circuit voltage (V_{oc}) were measured as shown in Fig. 2c–d and Fig. S5. It demonstrated the charges generation and charges transportation between the cloth vs PMMA and PVC, respectively. It was also observed that the output wave curve from the tribo-polarity reversal porous material could be regulated by the mechanical-structure design, where the charges on the porous surface presented in a suspending state as shown in Fig. 2d. Furthermore, the materials tribo-polarity provided a potential wave modulation solution using "1, 0, and −1″ in the view of electrical point as shown Figs. S6–S7.

2.3. Performance and optimization of DC-DTENG

A continuous DC output, V_{oc}, and transferred accumulative charges (Q_{tac}) from DC-DTENG in the measurement are as shown in Fig. 2e–g. The continuous DC and V_{oc} from electrode "A" were obtained of 45 nA and 149 V at a constant rotation of 60 rpm, and the Q_{tac} during a rotation cycle reached up to 47 nC. These electrical output curves demonstrated that the DC-DTENG presented a good DC output electrical characteristic. It is noted that the transition state light pink in the diagram meant the starting of rotation until the dynamic stability (light green) during the operation. It was also observed that a clockwise rotation and an anti-clockwise rotation did not affect the electrical output performance as shown in Fig. 2h–j (electrode "A" left-hand vs ground) and Fig. S8 (electrode "B" right-hand vs ground), respectively. The reason to explain this phenomenon is that the fixed positive and negative materials on both sides of the disk result in the transportation charges discharging
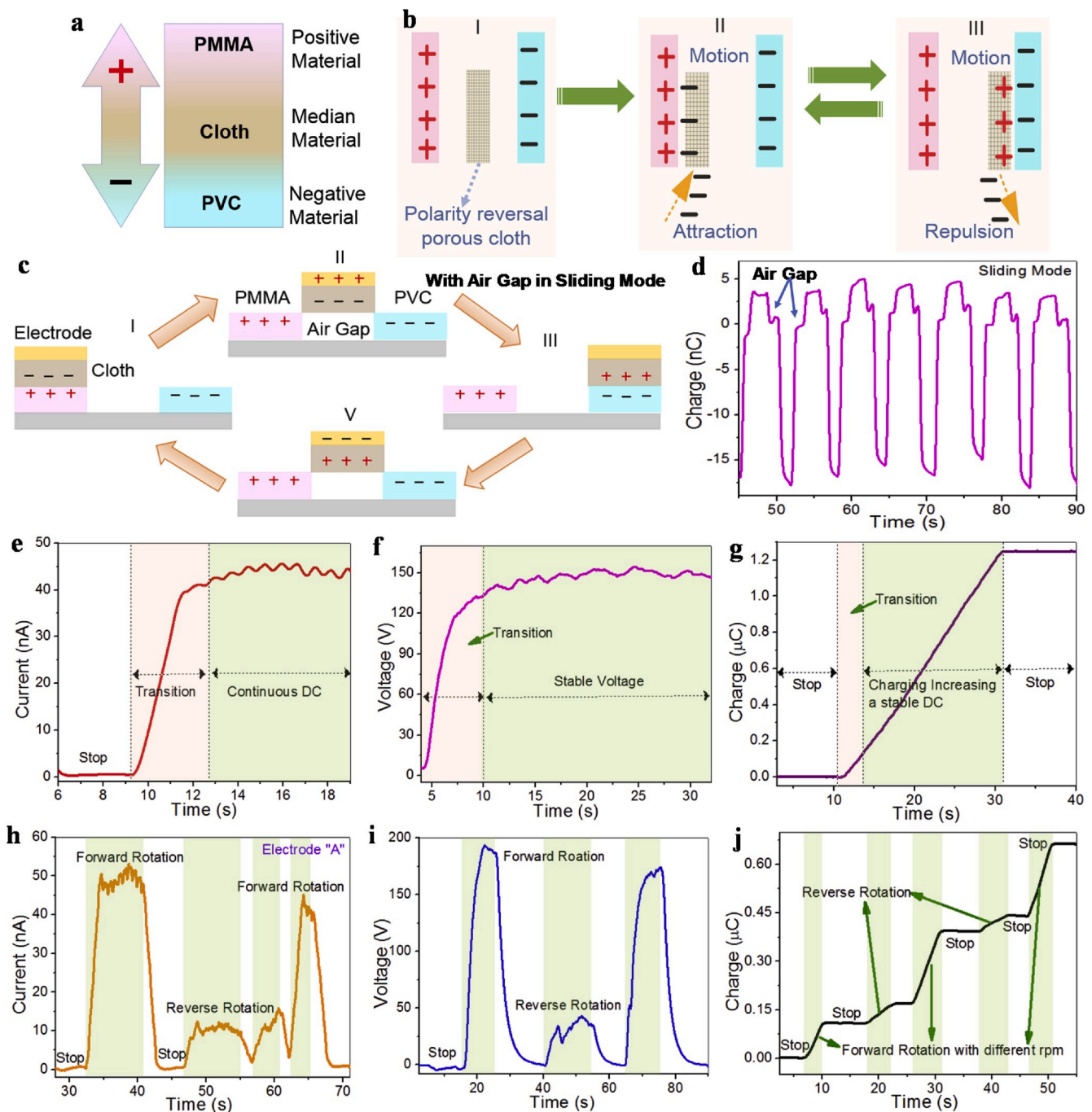
Fig. 2. Tribo-polarity materials and the output performance of DC-DTENG. (a) Induced charges distribution of three tribo-polarity materials: positive material PMMA, negative material PVC, and "median material" porous cloth. (b) The charges response phenomenon on the tribo-polarity reversal porous cloth "median material" between positive material and negative material. (c) Schematic graph of a sliding mode with an air gap between PMMA and PVC, and (d) transferred charges. (e) Continuous DC output, (f) V_{oc}, (g) transferred charges. (h–j) DC, V_{oc}, and Q_{tac} from the electrode "A" with different motion states.

onto line electrodes. The detail operation information of the DC output and those rotations were as shown in Video S1 Supplementary Information. Faster rotations to the rotator of DC-DTENG, a higher output DC was along with a higher V_{oc} and a steeper charges curve. To further investigate the theory of the DC-DTENG, a simplified electrical-mechanical system and its calculation analysis were as shown in Fig. 3. The momentary DC output was obtained by the derivative of the electrical charges with time. The current came from dual semi-independent TENG power sources, thus we had the following equation to electrode "A'" or electrode "B", respectively.
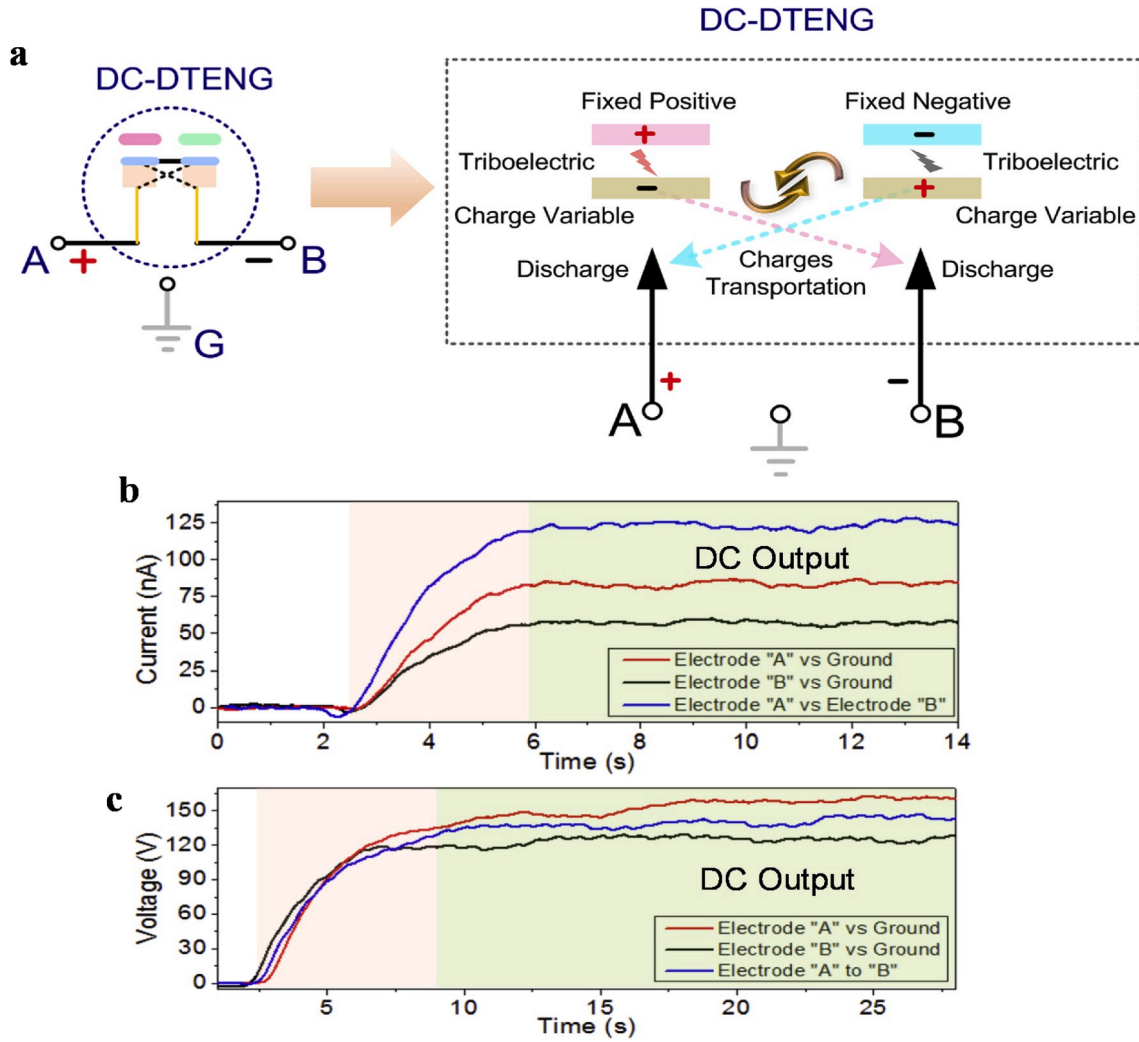
Supplementary video related to this article can be found at https

$$I_1 = \frac{\Delta Q_1}{\Delta t} \tag{1}$$

$$I_2 = \frac{\Delta Q_2}{\Delta t} \tag{2}$$

Here I_1 and I_2 were from the electrode "A" and electrode "B", respectively. Q_1 and Q_2 were from the accumulated charges from electrode "A" and electrode "B", respectively. Based on the test curve from Fig. 3b, DC I_{out} from electrode "A" and "B" was simplified as following,

Fig. 3. Simplified structure and theory analysis of the DC-DTENG. (a) It was observed that the DC-DTENG contained dual semi-independent TENG power sources. (b–c) Test output voltage and currents on electrodes vs ground, and DC output in all.

$$I_{out} = I_1 + I_2 \tag{3}$$

The output current from DC-DTENG was also from the coupling of the mechanical transportation charges on the disk, the charge releasing to both line electrodes and the charges generation from the PMMA and PVC. Thus, the output currents from both line electrodes were written as follows, respectively.

$$I_1 = \frac{\alpha Q_l W L}{t} = \alpha Q_l W v_r \tag{4}$$

$$I_2 = \frac{\beta Q_r W L}{t} = \beta Q_r W v_r \tag{5}$$

where α and β were the correction factors for line electrode "A" and "B", respectively. Q_l and Q_r were the generated charges from left-hand quarter PMMA and right-hand quarter PVC, respectively. W and L were the equivalent length and width of the triboelectric contact area, respectively. v_r was a rotational speed of a disk in DC-DTENG. Based on the test V_{oc} from Fig. 3c, the voltage from electrode "A" V_1 and "B" V_2 were simplified as following,

$$V_{out} = (V_1 + V_2)/2 \tag{6}$$

It concluded that the dual TENG worked independently as a DC power source. It was also found that the overall current from electrode "A" to electrode "B" was assumed a simplified sum of both currents

(electrode "A" vs ground, electrode "B" vs ground), whereas the voltage was calculated using the average value of the dual independent power sources in DC-DTENG. The test result confirmed this conclusion: the total output of 125 nA was the sum of the independent current output of two terminals "A" and "B", which were 50 nA and 75 nA.

DC output from DC-DTENG strongly relied on the relative rotation between the rotator and two stators. To reveal the physical relationship of the rotational rate and its output electrical performance, the value of Q_{tac} was used to identify different rotational speeds. Fig. 4a depicts a schematic diagram of the measurement points (electrode "A" vs ground and electrode "B" vs ground) in DC-DTENG, and the Q_{tac} with different rotations under two measurement points were obtained in Fig. 4b and c. It was found that faster rotations, the more accumulative charges were obtained within a limit time period. It was also found that 1.2 times more charges were obtained from electrode "A" compared to electrode "B". The reason was from materials PVC and PMMA. The porous "median material" cloth obtained more charges from PVC than a loss of charges from PMMA. To figure out the influence of the electrode location, Fig. 4d and e depicted the Q_{tac} with an asymmetric electrode (30° difference). It was observed that the electrode location decreased Q_{tac}. Meanwhile, with a smaller dimension of DC-DTENG (0.6 time's dimension), almost 0.6 times electrical output was obtained in our observation as shown in Fig. 4f and g. Fig. 4h–i and Fig. S9 described a DC, V_{oc}, and Q_{tac} of those schematic diagrams, respectively. The different values of the curves meant different rotations and with good recovery
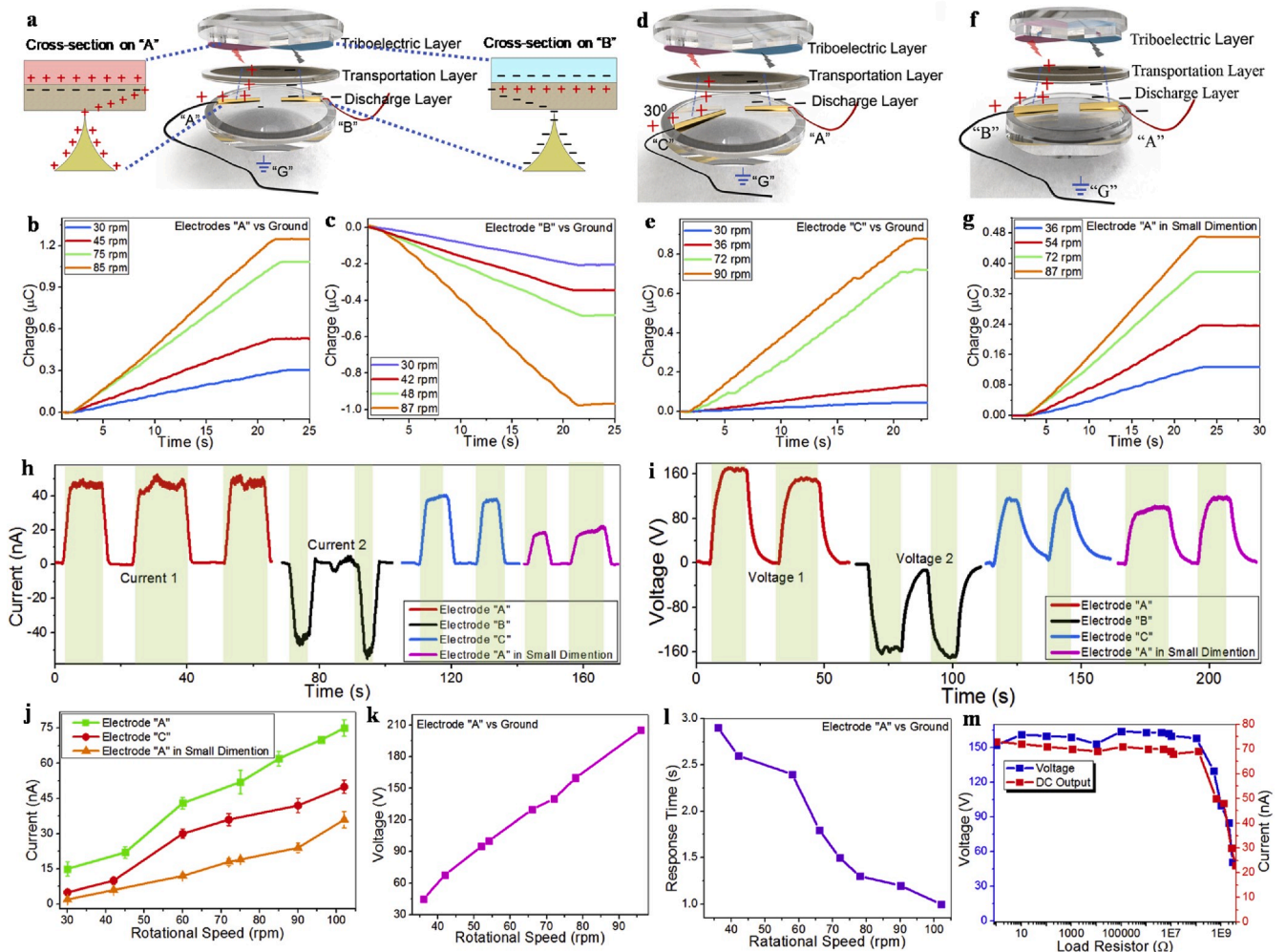
Fig. 4. Performance analysis and optimization of DC-DTENG. (a–c) Measurement points of the schematic diagram, and Q_{tac} under different rotational speeds. (d–e) Line electrode location schematic diagram and its Q_{tac} with different rotational speeds. (f–g) Schematic diagram of a smaller dimensional structure, and its Q_{tac} with different rotational speeds. (h–i) DC output and V_{oc} for those designed structures. (j–i) DC, V_{oc}, and response time in different rotations. (m) DC output current and V_{oc} with various external loads.

performance. In general, we observed that faster rotations, higher output current and V_{oc} were generated as shown in Fig. 4j and k. We also found that the voltage increased along with the faster rotations, while the response decreased. Applying different external loads to the DC-DTENG, the continuous output DC and V_{oc} were shown in Fig. 4m. Correspondingly, the load voltage vs different loads was in Fig. S10 which provided a reference for engineering applications. In addition, to demonstrate the durability as shown in Fig. S11, it observed that the output of DC-DTENG had almost no decreases after a long time (~12 min) operation in charge transportation.

2.4. Application for next-generation IoT in directly power in actuator and sensor

Electrical elements including actuators and sensors are playing a more and more important role in IoT. Switch "on" and "off" was one of the most critical devices in an electrical system. It was commonly used to improve the outcome of electrical performance and to drive a control electrical system. Fig. 5a–c demonstrated a soft switch application with a tip-plate configuration (~2 mm gap) driven by the DC-DTENG. It was demonstrated that the "on" and "off" behavior did not need any extra circuit and power to drive. As shown in Fig. 5a, when the DC flowed into the copper plate, the copper tip did a quick mechanical movement due to the electrostatic force. The "on" and "off" of the vibration soft switch

was characterized by the measurement data as shown in Fig. 5b–c and Fig. S12. Furthermore, Video S2 Supplementary Information demonstrated the evidence of the contact and separation between soft tip and plate. The peaks in the curve meant that the soft tip instantaneous contacted with the copper plate "on". As to the sensing application using DC-DTENG, a UV light radiation sensing application was shown in Fig. 5d–f. The mechanism of UV light activation electrons was as shown in Fig. 5d. When UV light radiations onto a metal film, the electrons on the metal film became more active. A UV light source (10–400 nm, 4 W power source) was as shown in Fig. S13a. When UV radiation lights were shining onto the DC-DTENG (Fig. 5e), a comparative higher current was observed. The explanation was that the UV radiation light resulted in more active electrons on the bottom electrode, which increased the DC output 12.3% more than without any UV light radiation (Fig. S13b Supplementary Information).

To broaden its applications in IoT using sensor nodes networks, a Bluetooth module powering by DC-DTENG for temperature and humidity sensing application was carried out as shown in Video S3 Supplementary Information. The electrical circuit of the connection with the module for the next-generation IoT was as shown in Fig. 5g. The charging and discharging curve were as shown in Fig. 5h, where each voltage drops from ~8 V to ~2.7 V representing a discharging to the Bluetooth module. It is noted that the first discharging was used to power the Bluetooth module, whereas the second discharging sent the
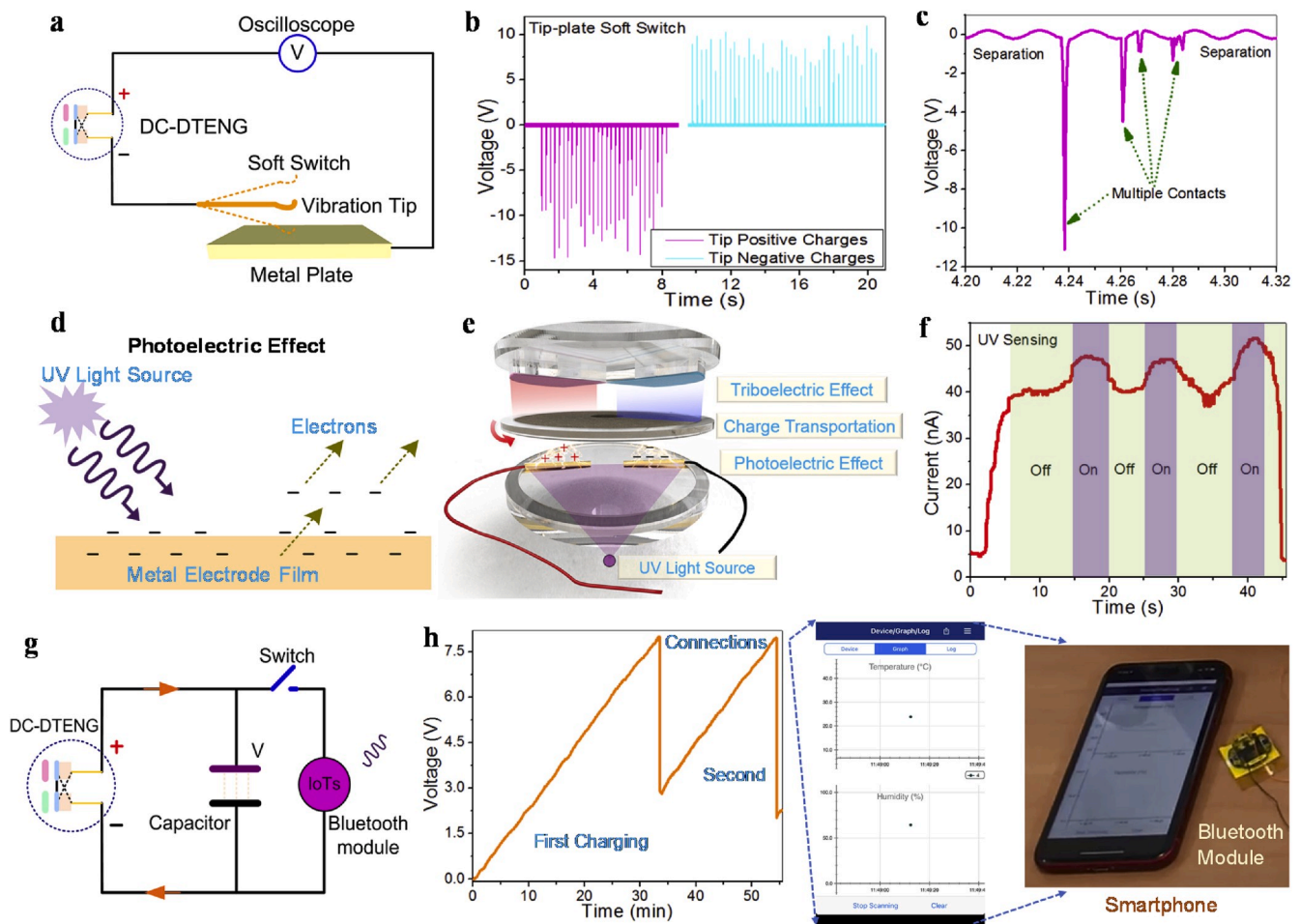
Fig. 5. Application of DC-DTENG for sensor, actuator, and next-generation IoT. (a) Schematic electrical-mechanical diagram of a soft switch application driven by DC-DTENG, (b) "on" and "off" verification by output voltage from an oscilloscope, and (c) zoom-in of a voltage curve to show the contact and separation of the "on" and "off" to the tip-plate configuration. (d) Mechanism of photoelectric effect by UV light radiation, (e) a UV light source was shining onto DC-DTENG, and (f) a UV sense is driven by the DC-DTENG. (g) Simplified circuit diagram of the DC-DTENG for powering next-generation IoT. (h) Charging and discharging curves with Bluetooth module driven by DC-DTENG for IoT application.

temperature of 26 °C and humidity of 65% to a smartphone to record.

Supplementary video related to this article can be found at https ://doi.org/10.1016/j.nanoen.2020.104760

2.5. Application for energy storage

Beyond the demonstration of the actuator and sensor, energy storage is vitally important to power electronic devices. As shown in Fig. 6a–c and Fig. S14, we observed that the electrode "A" vs electrode "B" increased the charging rate dramatically. The reason for this phenomenon was the dual semi-independent TENG power source operation in the same period. Meanwhile, the charging ability of the "B" electrodes presented a 1.5 time's charging rate than the "A" electrode. The cloth presented more positive charges when separated with PVC film (top fixed layer, right-hand), whereas it obtained fewer negative charges when separated with PMMA film (top fixed layer, left-hand). We observed that the electrode "A" vs electrode "B" dramatically increased the charging rate (almost 2 times) than a single electrode connection. The reason for this phenomenon was the dual semi-independent TENG power source in operation at the same time. Meanwhile, the charging ability of the "B" electrode presented a 1.5 time's charging rate than the "A" electrode. We assumed that the cloth presented more positive charges when separated with PVC film (top fixed layer, right-hand), whereas it obtained fewer negative charges when separated with PMMA film (top fixed layer, left-hand). The ability of the continuous DC

output enables the DC-DTENG to charge energy storage devices directly without any rectifier unit as shown in Fig. 6d. The charge rate with different rotations was as shown in Fig. 6e. It was observed that the faster rotations increased the charge rate into the capacitor. It was also observed that the DC-DTENG charged up to 4 V to 1 µF within 75 s by a DC-DTENG as shown in Fig. 6f. For a higher DC output, the array pairs of dielectrics were designed to demonstrate the enhancement of DC output. As shown in Fig. 6g–h and Fig. S15, it was observed a mathematical relationship between the pairs of arrays vs the DC output, such as two pairs of 1.8 times DC output, three pairs of 2.8 times, and four pairs dielectrics (PMMA and PVC) of 3.6 time's DC output. Moreover, we observed a consistent current polarity output (the same for both clockwise and anti-clockwise rotation in random direction wind) from the DC-DTENG, which is a big advantage for a realistic application than any other existing mechanisms for power generation. With those demonstrations on array pairs dielectrics (n number on a plane) and multi-layers (m layers on volume) of DC-DTENG installation into an independent smart home system, the DC-DTENGs with a certain number (p) could be driven by natural wind flow as shown in Fig. 6j. In addition, it could easily obtain enough power, and even drive all kinds of actuators and sensor units in a potential smart home application using the DC-DTENGs.
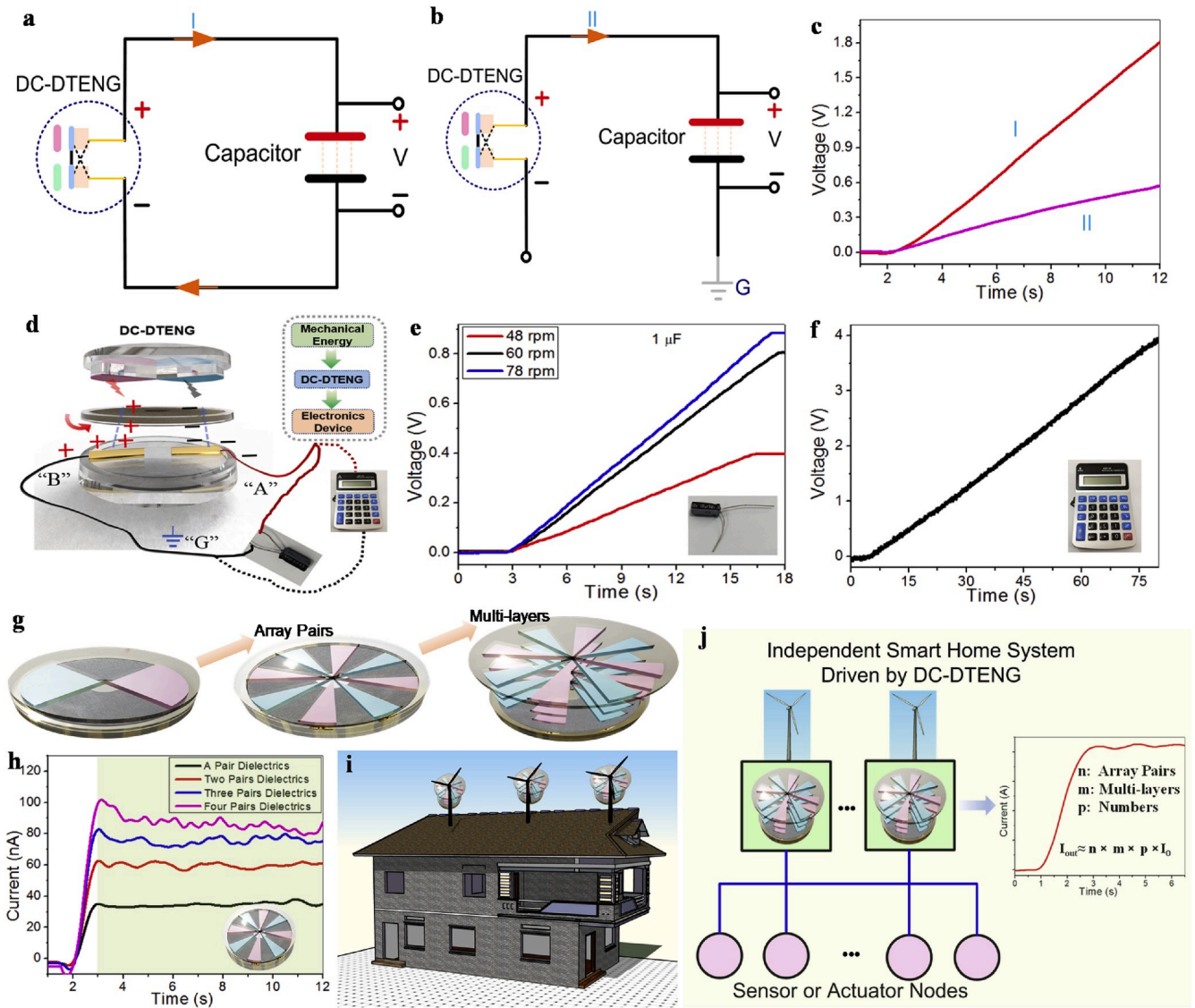
Fig. 6. DC-DTENG as energy storage and its potential as a higher output. (a) Schematic charging electrical diagram using electrode "A" and "B", (b) schematic charging electrical diagram using electrode "A", and (c) measurement voltage vs time on capacitor for two connection methods. (d) System diagram of DC-DTENG to directly power an electronic device. (e) The charge rates of 1 μF capacitor with different rotations, and (f) the charges vs time to demonstrate the charging capability for a commercial device. (g) A way to increase DC output using array pairs "n" (plane) and multi-layers dielectrics "m" (volume). The DC output of DC-DTENG increased using the more array pairs in-plane and the multi-layers in stacks. (h) Test DC outputs from an array DC-DTENG and (i) A potential smart home system application of DC outputs driven by random wind rotation on its roof. It was noted that the wind rotation direction did not affect the DC output performance of DC-DTENGs. (j) The potential electrical diagram of the potential smart home system for sensor and actuator driven by DC-DTENG.

2.6. Application for next-generation VR in real-time monitoring and continuous control

The human-machine interface using triboelectric normally defines "0" and "1" states with discontinuous characteristic information identifications stimulations (e.g. frequency, number of peaks, absolute value range). With those definitions in the virtual space, it is almost impossible to reach continuous motion control in conventional TENG due to the superfast charges in a generation. However, almost all the things in the real space and virtual space are relating to the time-continuous, such as human motion behavior, games, and sports activities, etc. Thus, to achieve continuous motion control and real-time monitoring, we first time successfully realized scenario applications by DC-DTENG for the next-generation continuous VR motion control using triboelectric in both real space and virtual space. The reason for the real-time motion control of DC-DTENG was from the rotational speed during the process of charge transportation. With higher rotational speed, the higher

output voltage and current would be generated resulting in a numerical relationship of them. More detail in VR application, DC-DTENG prototype in real space was directly connected with the pre-processing circuit and micro control unit (MCU) to control the virtual activities in virtual space as shown in Fig. 7a and b. The pre-processing circuit was used to collect the continuous DC output signal which contained mechanical activities information from DC-DTENG, such as the rotational speed, frequency, and motion behaviors. The sampling frequency of the A/D converter is enough to capture the real-time motion status in real space and the precision of acquisition voltage reached up to 0.01 V. The MCU is connected to the USB port of a computer. Together with "Unity3D" by Unity Technologies and C++ programming language, the virtual space was built for a rotation disk monitoring and racing game experiments. The real-time mechanical activity information of the DC-DTENG in real space can be well monitored in the virtual space with the real-time display as shown in Fig. 7c and d and Video S4 Supplementary Information. It notes that we used the MCU (Arduino) to acquire the data
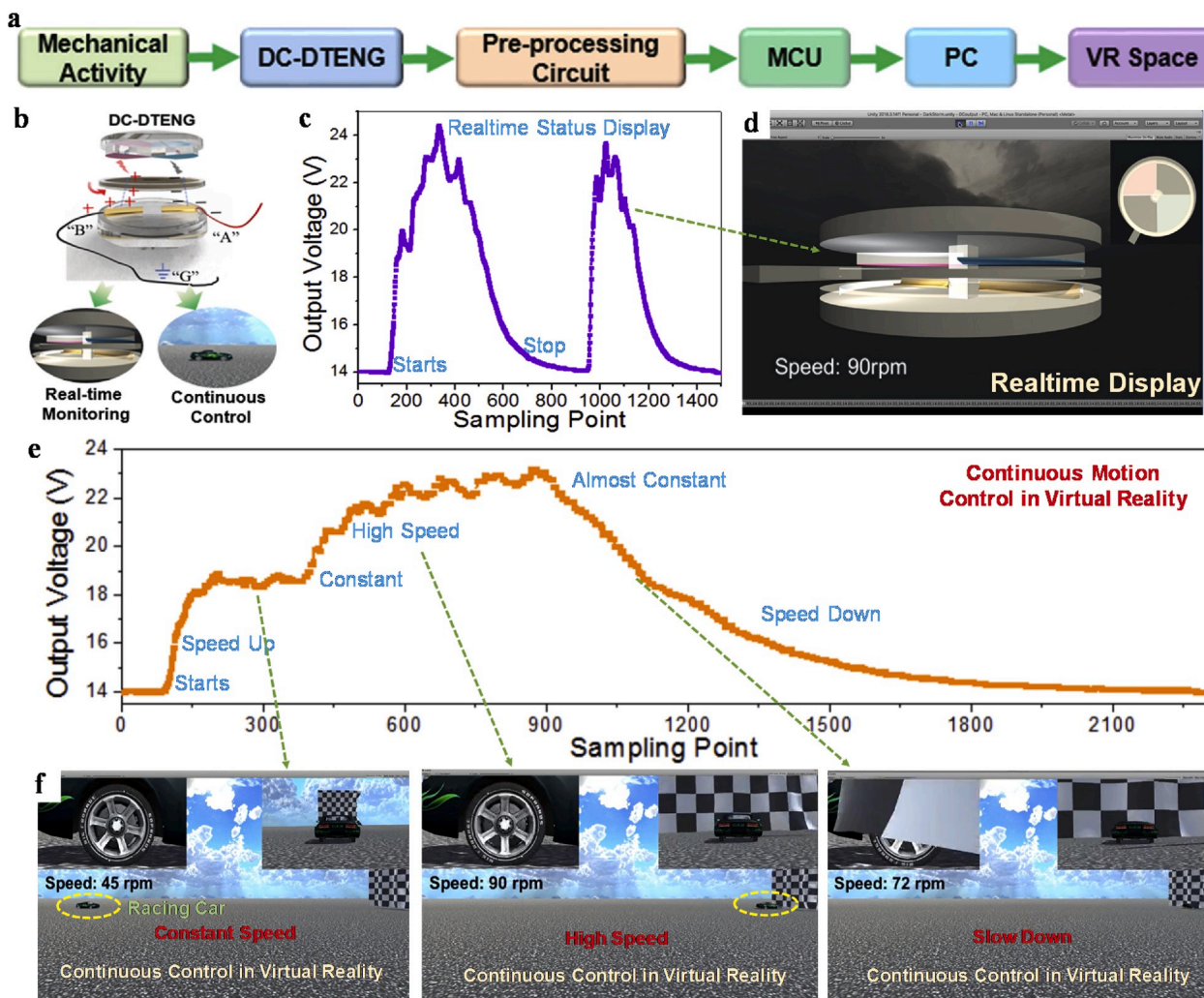
Fig. 7. Application of DC-DTENG in real-time monitoring and continuous motion control for next-generation VR. (a) Flow diagram for next-generation real-time VR. (b) Schematic diagram using DC-DTENG for VR applications. (c) Real-time status of the voltage curve by DC-DTENG for display monitoring, and (d) the rotational disk in virtual space. (e) Voltage curve in a racing game to demonstrate continuous motion control, and (f) the racing game in virtual space in constant speed, high speed, and speed slow down.

point with the baud rate 9600 Baud/s. Here, the sampling rate in our measurement are about 100 Point/s. To demonstrate the continuous VR motion control using DC-DTENG, a racing game in virtual space was further successfully conducted as shown in Fig. 7e and f and Video S5 Supplementary Information. It can clearly identify that the continuous control in speed up, constant speed, speed further up, and speed down is presenting in a real-time connection with the real space and the virtual space. It is also noted that the racing car in virtual space is totally controlled by the corresponding continuous output signals from the real DC-DTENG with mechanical activities.

Supplementary video related to this article can be found at https ://doi.org/10.1016/j.nanoen.2020.104760

3. Conclusions

In summary, we proposed a novel triboelectric mechanism using dual intersection TENGs and charge transportation for DC output to directly power the next-generation self-sustained IoT and its real-time control in VR. Just like the water transported by a waterwheel or P–N junction diode, we employed tribo-polarity reversal porous material as charges transportation carrier sliding among the ultra-negative and ultra-positive dielectric materials, and the charges were continuous unidirectional transported and repelled discharge onto electrodes for DC

output without a rectifier bridge. Due to charges transportation and discharge of repulsion, the DC output voltage of DC-DTENG was obtained up to ~5 times higher than the air breakdown in conventional TENG, and the charging rate reached up to 2 times higher than that of a TENG with the same materials, respectively. More interesting, the consistent current polarity (the same for both clockwise and anticlockwise rotation) of the DC-DTENG provided room for a realistic application, such as wind flow in a random direction. Moving forward the real applications by DC-DTENG, we demonstrated the realistic applications of a soft switch actuator, UV radiation sensing, and energy storage for an electronic device. We also successfully carried out a wireless Bluetooth module directly transmitting sensor nodes signals to a smartphone for next-generation IoT to directly power sensor nodes applications. Furthermore, to overcome the discontinuous characteristic identification (e.g. frequency, number of peaks, absolute value range) in the triboelectric, we first time successfully provided a practical solution for next-generation VR in real-time monitoring and continuous motion control between the real space and the virtual space.

4. Experimental section

Fabrication of the DC-DTENG: The rotator disk was made of porous cloth. The "median material" cloth (sliding layer) was assembled with an

acrylic ring (2 cm width, 22 cm outer and 20 cm inner diameter). The dimension of the porous cloth disk was designed with a 20 cm diameter. A pair of dielectrics was attached to the top layer stator. The materials of pair dielectrics were PMMA and PVC, respectively. The PMMA dielectric presented positive surface charges contacting with cloth (negative charges), whereas the PVC dielectric exhibited negative surface charges to cloth (positive charges) in operation. The PMMA film was located on the left-hand side with a quarter area of the disk, and the PVC was located on the right-hand side with another quarter area of the disk. The bottom electrode "A" and "B" were line electrodes placed at the bottom stator. The line electrodes were made of cloth which coated with nickel metal. The length dimension was 4 cm in our device. The reason for choosing this electrode was its mechanical property with enough flexibility and easy integration to our device. The substrate of the device was made of an acrylic plate which was cut by a laser cutting machine. The small dimension of DC-DTENG was with a scale of 0.6 times its original one.

COMSOL simulation: The potential and charges distribution on the rotational disk had been obtained from a Finite Element Analysis (FEA) simulation with COMSOL Multiphysics 4.2. The models were built with approximately 1296 2D solid elements with a step size 0.94. The rotational disk was surrounded by air, which was the same as the usual case in the experiment. The potential at infinity was chosen as the reference point for the electric potential, which was 0. The disk material cloth (polyester) property was assigned in the COMSOL software. The instantaneous changes density in the space on the disk surface was chosen as 50e-6 C/m^3 at the bottom and $-50e-6$ C/m^3 at a top for our FEA calculation, respectively.

Characterization: A programmable electrometer (Keithley model 6514) was used to obtain the V_{oc}, DC output, and Q_{tac}, respectively. The rotational speed of DC-DTENG was calculated using a stopwatch. The output voltage of the measurement for the soft switch was tested by an oscilloscope (Keysight, DSOX3034T) with an internal resistance 50 Ω, and the high precision current equipment (Stanford Research System, Model SR570) was used for the measurement of the DC output.

Declaration of competing interest

The authors declare that they have no known competing financial interests or personal relationships that could have appeared to influence the work reported in this paper.

CRediT authorship contribution statement

Jianxiong Zhu: Conceptualization, Data curation, Formal analysis, Investigation, Methodology, Validation, Writing - original draft, Writing - review & editing. **Hao Wang:** Conceptualization, Data curation, Formal analysis, Investigation, Methodology, Validation, Writing - original draft. **Zixuan Zhang:** Conceptualization, Data curation, Investigation, Methodology, Validation, Writing - original draft, Writing - review & editing. **Zhihao Ren:** Methodology, Validation, Writing - original draft. **Qiongfeng Shi:** Methodology. **Weixin Liu:** Data curation. **Chengkuo Lee:** Conceptualization, Funding acquisition, Investigation, Methodology, Supervision, Validation, Writing - original draft, Writing - review & editing.

Acknowledgements

Appendix A. Supplementary data

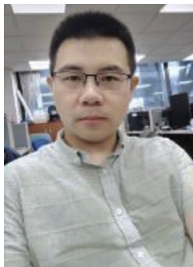Supplementary data to this article can be found online at https://doi.org/10.1016/j.nanoen.2020.104760.

References

[1] M. Zidan, J. Strachan, W. Lu, The future of electronics based on memristive systems, Nat. Electron. 1 (2018) 22.

[2] Y. Zhan, Y. Mei, L. Zheng, Materials capability and device performance in flexible electronics for the internet of things, J. Mater. Chem. C. 2 (2014) 1220.

[3] A. Yu, X. Chen, R. Wang, J. Liu, J. Luo, L. Chen, Y. Zhang, W. Wu, C. Liu, H. Yuan, M. Peng, W. Hu, J. Zhai, Triboelectric nanogenerator as a self-powered communication unit for processing and transmitting information, ACS Nano 10 (2016) 3944.

[4] H. Guo, X. Pu, J. Chen, Y. Meng, M. Yeh, G. Liu, Q. Tang, B. Chen, D. Liu, S. Qi, C. Wu, C. Hu, J. Wang, Z.L. Wang, A highly sensitive, self-powered triboelectric auditory sensor for social robotics and hearing aids, Sci. Robot 3 (2018) 2516.

[5] X. Wang, J. Song, J. Liu, Z.L. Wang, Direct-current nanogenerator driven by ultrasonic waves, Science 316 (2007) 102.

[6] R. Stark, K. Schoenbach, Direct current high-pressure glow discharges, J. Appl. Phys. 85 (1999) 2075.

[7] G. Cheng, H. Zheng, F. Yang, L. Zhao, M. Zheng, J. Yang, H. Qin, Z. Du, Z.L. Wang, Managing and maximizing the output power of a triboelectric nanogenerator by controlled tip–electrode air-discharging and application for UV sensing, Nano Energy 44 (2018) 208.

[8] J. Cheng, W. Ding, Y. Zi, Y. Lu, L. Ji, F. Liu, C. Wu, Z.L. Wang, Triboelectric microplasma powered by mechanical stimuli, Nat. Commun. 9 (2018) 3733.

[9] A. Li, Y. Zi, H. Guo, Z.L. Wang, F.M. Fernandez, Triboelectric nanogenerators for sensitive nano-coulomb molecular mass spectrometry, Nat. Nanotechnol. 12 (2017) 481.

[10] J. Yang, F. Yang, L. Zhao, W. Shang, H. Qin, S. Wang, X. Jiang, G. Cheng, Z. Du, Managing and optimizing the output performances of a triboelectric nanogenerator by a self-powered electrostatic vibrator switch, Nano Energy 46 (2018) 220.

[11] H. Chen, L. Miao, Z. Su, Y. Song, M. Han, X. Chen, X. Cheng, D. Chen, H. Zhang, Fingertip-inspired electronic skin based on triboelectric sliding sensing and porous piezoresistive pressure detection, Nano Energy 40 (2017) 65.

[12] S. Niu, X. Wang, F. Yi, Y. Zhou, Z.L. Wang, A universal self-charging system driven by random biomechanical energy for sustainable operation of mobile electronics, Nat. Commun. 6 (2015) 8975.

[13] H. Yang, Y. Pang, T. Bu, W. Liu, J. Luo, D. Jiang, C. Zhang, Z.L. Wang, Triboelectric micromotors actuated by ultralow frequency mechanical stimuli, Nat. Commun. 10 (2019) 2309.

[14] H. Ryu, J. Lee, U. Khan, S. Kwak, R. Hinchet, S. Kim, Sustainable direct current powering a triboelectric nanogenerator via a novel asymmetrical design, Energy Environ. Sci. 11 (2018) 2057.

[15] A. Fischer, A. Allerman, M. Crawford, K. Bogart, S. Lee, R. Kaplar, W. Chow, S. Kurtz, Fullmer, Room-temperature direct current operation of 290 nm light-emitting diodes with milliwatt power levels, J. Appl. Phys. Lett. 84 (2004) 3394.

[16] V. Pribiag, I. Krivorotov, G. Fuchs, P. Ozatay, J. Sankey, D. Ralph, R. Buhrman, Magnetic vortex oscillator driven by d.c. spin-polarized current, Nat. Phys. 3 (2007) 498.

[17] F. Fan, Z. Tian, Z.L. Wang, Flexible triboelectric generator, Nano Energy 1 (2012) 328.

[18] S. Wang, L. Lin, Z.L. Wang, Triboelectric nanogenerators as self-powered active sensors, Nano Energy 11 (2015) 436.

[19] C. Zhang, Z.L. Wang, Tribotronics—a new field by coupling triboelectricity and semiconductor, Nano Today 11 (2016) 521.

[20] G. Zhu, J. Chen, T. Zhang, Q. Jing, Z.L. Wang, Radial-arrayed rotary electrification for high performance triboelectric generator, Nat. Commun. 5 (2014) 3426.

[21] W. Seung, M. Gupta, K. Lee, K. Shin, J. Lee, T. Kim, S. Kim, J. Lin, J. Kim, S. Kim, Nanopatterned textile-based wearable triboelectric nanogenerator, ACS Nano 9 (2015) 3501.

[22] J. Zhong, Q. Zhong, F. Fan, Y. Zhang, S. Wang, B. Hu, Z.L. Wang, J. Zhou, Finger typing driven triboelectric nanogenerator and its use for instantaneously lighting up LEDs, Nano Energy 2 (2013) 491.

[23] T. Zhou, Z. Yang, Y. Pang, L. Xu, C. Zhang, Z.L. Wang, Tribotronic tuning diode for active analog signal modulation, ACS Nano 11 (2017) 882.

[24] Y. Zi, J. Wang, S. Wang, S. Li, Z. Wen, H. Guo, Z.L. Wang, Effective energy storage from a triboelectric nanogenerator, Nat. Commun. 7 (2015) 10987.

[25] J. Wang, T. He, C. Lee, Development of neural interfaces and energy harvesters towards self-powered implantable systems for healthcare monitoring and rehabilitation purposes, Nano Energy 65 (2019) 104039.

[26] J. Wang, H. Wang, N. Thakor, C. Lee, Self-powered direct muscle stimulation using a triboelectric nanogenerator (TENG) integrated with a flexible multiple-channel intramuscular electrode, ACS Nano 13 (2019) 3589–3599.

[27] S. Lee, W. Peh, J. Wang, F. Yang, J. Ho, N. Thakor, S. Yen, C. Lee, Toward bioelectronic medicine neuromodulation of small peripheral nerves using flexible neural clip (FNC), Adv. Sci. 2017 (2017) 1700149.

[28] T. Chen, Q. Shi, M. Zhu, T. He, L. Sun, L. Yang, C. Lee, Triboelectric self-powered wearable flexible patch as 3D motion control interface for robotic manipulator, ACS Nano 12 (2018) 11561–11571.

[29] S. Niu, Y. Liu, S. Wang, L. Lin, Y. Zhou, Y. Hu, Z.L. Wang, Theory of sliding-mode triboelectric nanogenerators, Adv. Mater. 25 (2013) 6184.

[30] S. Niu, Z.L. Wang, Theoretical systems of triboelectric nanogenerators, Nano Energy 14 (2015) 161.

[31] Y. Kwon, S. Shin, Y. Kim, J. Jung, M. Lee, J. Nah, Triboelectric contact surface charge modulation and piezoelectric charge inducement using polarized composite thin film for performance enhancement of triboelectric generators, Nano Energy 25 (2016) 225.

[32] G. Zhu, C. Pan, W. Guo, C. Chen, Y. Zhou, R. Yu, Z.L. Wang, Triboelectric-generator-driven pulse electrodeposition for micropatterning, Nano Lett. 12 (2012) 4960.

[33] C. Qiu, F. Wu, Q. Shi, C. Lee, M. Yuce, Sensors and control interface methods based on triboelectric nanogenerator in IoT applications, IEEE Access 7 (2019) 92745–92757.

[34] Q. Shi, C. Lee, Self-powered bio-inspired spider-net-coding interface using single-electrode triboelectric nanogenerator, Adv. Sci. 6 (2019) 1900617.

[35] M. Zhu, Q. Shi, T. He, Z. Yi, Y. Ma, B. Yang, T. Chen, C. Lee, Self-powered and self-functional cotton sock using piezoelectric and triboelectric hybrid mechanism for healthcare and sports monitoring, ACS Nano 13 (2019) 1940–1952.

[36] F. Hassani, W. Peh, G. Gammad, R. Mogan, T. Ng, T. Kuo, L. Ng, P. Luu, S. Yen, C. Lee, A three-dimensionally (3D) printed implantable device for voiding the bladder using shape memory alloy (SMA) actuators, Adv. Sci. 2017 (2017) 1700143.

[37] X. Cheng, L. Miao, Y. Song, Z. Su, H. Chen, X. Chen, J. Zhang, H. Zhang, High efficiency power management and charge boosting strategy for a triboelectric nanogenerator, Nano Energy 38 (2017) 438.

[38] J. Chun, B.U. Ye, J. Lee, D. Choi, C. Kang, S. Kim, Z.L. Wang, J. Bail, Boosted output performance of triboelectric nanogenerator via electric double layer effect, Nat. Commun. 7 (2016) 12985.

[39] G. Cheng, Z. Lin, L. Lin, Z. Du, Z.L. Wang, Pulsed nanogenerator with huge instantaneous output power density, ACS Nano 7 (2013) 7383.

[40] L. Luo, D. Bao, W. Yu, Z. Zhang, T.L. Ren, A low input current and wide conversion ratio buck regulator with 75% efficiency for high-voltage triboelectric nanogenerators, Sci. Rep. 6 (2016) 19246.

[41] J. Liu, A. Goswami, K. Jiang, F. Khan, S. Kim, R. McGee, Z. Li, Z. Hu, J. Lee, T. Thundat, Direct-current triboelectricity generation by a sliding Schottky nanocontact on MoS$_2$ multilayers, Nat. Nanotechnol. 13 (2018) 112.

[42] C. He, C. Han, G. Gu, T. Jiang, B. Chen, Z. Gao, Z.L. Wang, Hourglass triboelectric nanogenerator as a "direct current" power source, AdV. Energy Mater. 7 (2017) 1700644.

[43] J. Luo, L. Xu, W. Tang, T. Jiang, F.R. Fan, Y. Pang, L. Chen, Y. Zhang, Z.L. Wang, Direct-current triboelectric nanogenerator realized by air breakdown induced ionized air channel, AdV. Energy Mater. 8 (2018) 1800889.

[44] D. Liu, X. Yin, H. Guo, L. Zhou, X. Li, C. Zhang, J. Wang, Z.L. Wang, A constant current triboelectric nanogenerator arising from electrostatic breakdown, Sci. Adv. 5 (2019) 6437.

[45] H. Zou, Y. Zhang, L. Guo, P. Wang, X. He, G. Dai, H. Zheng, C. Chen, A. Wang, C. Xu, Z.L. Wang, Quantifying the triboelectric series, Nat. Commun. 10 (2019) 1427.

[46] Z.L. Wang, J. Chen, L. Lin, Progress in triboelectric nanogenerators as a new energy technology and self-powered sensors, Energy Environ. Sci. 8 (2015) 2250–2282.

[47] Z. Lin, J. Yang, X. Li, Y. Wu, W. Wei, J. Liu, J. Chen, J. Yang, Large-scale and washable smart textiles based on triboelectric nanogenerator arrays for selfpowered sleeping monitoring, Adv. Funct. Mater. 28 (2018) 1704112.

[48] J. Chen, W. Xuan, P. Zhao, U. Farooq, P. Ding, W. Yin, H. Jin, X. Wang, Y. Fu, S. Dong, Triboelectric effect based instantaneous self-powered wireless sensing with self-determined identity, Nano Energy 51 (2018) 1–9.

[49] K.-W. Lim, M. Peddigari, C.H. Park, H.Y. Lee, Y. Min, J.-W. Kim, C.-W. Ahn, J.-J. Choi, B.-D. Hahn, J.-H. Choi, A high output magneto-mechano-triboelectric generator enabled by accelerated water-soluble nano-bullets for powering a wireless indoor positioning system, Energy Environ. Sci. 12 (2019) 666–674.

[50] H. Wang, J. Wang, T. He, Z. Li, C. Lee, Direct muscle stimulation using diode amplified triboelectric nanogenerators (TENGs), Nano Energy 63 (2019) 103844.

[51] W. Yin, Y. Xie, J. Long, P. Zhao, J. Chen, J. Luo, X. Wang, S. Dong, A self-power transmission and non-contact-reception keyboard based on a novel resonant triboelectric nanogenerator (R-TENG), Nano Energy 50 (2018) 16–24.

[52] S.W. Chen, X. Cao, N. Wang, L. Ma, H.R. Zhu, M. Willander, Y. Jie, Z.L. Wang, An ultrathin flexible single-electrode triboelectric-nanogenerator for mechanical energy harvesting and instantaneous force sensing, Adv. Energy Mater. 7 (2017) 1601255.

[53] S. Park, S. Ahn, J. Sun, D. Bhatia, D. Choi, K.S. Yang, J. Bae, J.J. Park, Highly bendable and rotational textile structure with prestrained conductive sewing pattern for human Joint monitoring, Adv. Funct. Mater. 29 (2019) 1808369.

[54] M. Xu, P. Wang, Y.C. Wang, S.L. Zhang, A.C. Wang, C. Zhang, Z. Wang, X. Pan, Z. L. Wang, A soft and robust spring based triboelectric nanogenerator for harvesting arbitrary directional vibration energy and self-powered vibration sensing, Adv. Energy Mater. 8 (2018) 1702432.

[55] X. Wang, Y. Yang, Effective energy storage from a hybridized electromagnetictriboelectric nanogenerator, Nano Energy 32 (2017) 36–41.

[56] R. Hinchet, H.-J. Yoon, H. Ryu, M.-K. Kim, E.-K. Choi, D.-S. Kim, S.-W. Kim, Transcutaneous ultrasound energy harvesting using capacitive triboelectric technology, Science 365 (2019) 491–494.

[57] Y. Yang, N. Sun, Z. Wen, P. Cheng, H. Zheng, H. Shao, Y. Xia, C. Chen, H. Lan, X. Xie, Liquid-metal-based super-stretchable and structure-designable triboelectric nanogenerator for wearable electronics, ACS Nano 12 (2018) 2027–2034.

[58] Q. Shen, X. Xie, M. Peng, N. Sun, H. Shao, H. Zheng, Z. Wen, X. Sun, Self-powered vehicle emission testing system based on coupling of triboelectric and chemoresistive effects, Adv. Funct. Mater. 28 (2018) 1703420.

[59] Q. Shi, H. Wu, H. Wang, H. Wu, C. Lee, Self-powered gyroscope ball using a triboelectric mechanism, Adv. Energy Mater. 7 (2017) 1701300.

[60] J. Zhu, X. Liu, Q. Shi, T. He, Z. Sun, X. Guo, W. Liu, O. Sulaiman, B. Dong, C. Lee, Development trends and perspectives of future sensors and MEMS/NEMS, Micromachines 11 (2020) 541.

[61] T. He, H. Wang, J. Wang, X. Tian, F. Wen, Q. Shi, J. Ho, C. Lee, Self-sustainable wearable textile nano-energy nano-system (NENS) for next-generation healthcare applications, Adv. Sci. (2019) 1901437.

[62] T. Chen, M. Zhao, Q. Shi, Z. Yang, H. Liu, L. Sun, J. Ouyang, C. Lee, Novel augmented reality interface using a self-powered triboelectric based virtual reality 3D-control Sensor, Nano Energy 51 (2018) 162–172.

[63] J. Zhu, X.Y. Guo, D.H. Meng, M. Choi, I. Park, R. Huang, W.X. Song, A flexible comb electrode triboelectric-electret nanogenerator with separated microfibers for self-powered position, motion direction and acceleration tracking sensor, J. Mater. Chem. 6 (2018) 16548–16555.

[64] W.X. Song, J. Zhu, B.H. Gan, S.Y. Zhao, H. Wang, C.J. Li, J. Wang, Flexible, stretchable, and transparent planar Microsupercapacitors based on 3D porous laser-induced graphene, Small (2017) 1702249.

[65] J. Zhu, Y.L. Zhu, W.X. Song, H. Wang, M. Gao, M. Cho, I. Park, Zinc oxide enhanced piezoelectret polypropylene microfibers for mechanical energy harvesting, ACS Appl. Mater. Interfaces 10 (2018) 19940–19947.

[66] T.X. Xiao, T. Jiang, J. Zhu, X. Liang, L. Xu, J.J. Shao, J. Wang, Z.L. Wang, Silicone-based triboelectric nanogenerator for water wave energy harvesting, ACS Appl. Mater. Interfaces 10 (2018) 3616–3623.

[67] B. Zhang, J. Chen, L. Jin, W. Deng, L. Zhang, H. Zhang, M. Zhu, W. Yang, Z. L. Wang, Rotating-disk-based hybridized electromagnetic–triboelectric nanogenerator for sustainably powering wireless traffic volume sensors, ACS Nano 10 (2016) 6241–6247.

[68] H. Wang, Z. Xiang, P. Giorgia, X. Mu, Y. Yang, Z.L. Wang, C. Lee, Triboelectric liquid volume sensor for self-powered lab-on-chip applications, Nano Energy 23 (2016) 80–88.

[69] S. Lee, S. Yen, S. Sheshadri, I. Martinez, N. Xue, Z. Xiang, N. Thakor, C. Lee, Flexible epineural strip electrode (FLESE) for recording in fine nerves, IEEE Trans. Biomed. Eng. 63 (2016) 581–587.

[70] L. Dhakar, S. Gudla, X. Shan, Z. Wang, F. Tay, C. Heng, C. Lee, Large scale triboelectric nanogenerator and self-powered pressure sensor array using low cost roll-to-roll UV embossing, Sci. Rep. 6 (2016) 22253.

[71] L. Dhakar, P. Pitchappa, F. Tay, C. Lee, An intelligent skin based self-powered finger motion sensor integrated with triboelectric nanogenerator, Nano Energy 19 (2016) 532–540.

[72] H. Qin, G. Cheng, Y. Zi, G. Gu, B. Zhang, W. Shang, F. Yang, J. Yang, Z. Du, Z. L. Wang, High energy storage efficiency triboelectric nanogenerators with unidirectional switches and passive power management circuits, Adv. Funct. Mater. 28 (2018) 1805216.

[73] B. Doyle, P. Peercy, Technique for profiling ^{1}H with 2.5-MeV van de Graaff accelerators, Appl. Phys. Lett. 34 (1979) 811.

[74] S. Bashkin, Optical spectroscopy with Van de Graaff accelerators, Nucl. Instrum. Methods 28 (1964) 88–96.

[75] H. Oona, W. Bickel, Modification of a Van de Graaff ion source to accelerate metal elements, Rev. Sci. Instrum. 47 (1976) 517.

[76] Z. Wu, W. Ding, Y. Dai, K. Dong, C. Wu, L. Zhang, Z. Lin, J. Cheng, Z.L. Zhang, Self-powered multifunctional motion sensor enabled by magnetic-regulated triboelectric nanogenerator, ACS Nano 12 (2018) 5726–5733.

[77] Y. Zi, C. Wu, W. Ding, X. Wang, Y. Dai, J. Cheng, J. Wang, Z. Wang, Z.L. Wang, Field emission of electrons powered by a triboelectric nanogenerator, Adv. Funct. Mater. 28 (2018) 1800610.

[78] C. Wu, H. Tetik, J. Cheng, W. Ding, H. Guo, X. Tao, N. Zhou, Y. Zi, Z. Wu, H. Wu, D. Lin, Z.L. Wang, Electrohydrodynamic jet printing driven by a triboelectric nanogenerator, Adv. Funct. Mater. 29 (2019) 1901102.

[79] W. Ding, J. Zhou, J. Cheng, Z. Wang, H. Guo, C. Wu, S. Xu, Z. Wu, X. Xie, Z. L. Wang, Tribo pump: a low-cost, hand-powered water disinfection system, Adv. Energy Mat. 9 (2019) 1901320.

[80] H. Huo, F. Liu, Y. Luo, Q. Gu, Y. Liu, Z. Wang, R. Chen, L. Ji, Y. Lu, R. Yao, J. Cheng, Triboelectric nanogenerators for electro-assisted cell printing, Nano Energy 67 (2020) 104150.

[81] L. Zhao, H. Li, J. Meng, A. Wang, P. Tan, Y. Zou, Z. Yuan, J. Lu, C. Pan, Y. Fan, Y. Zhang, Y. Zhang, Z.L. Wang, Z. Li, Reversible conversion between Schottky and ohmic contacts for highly sensitive, multifunctional biosensors, Adv. Funct. Mater. 30 (2020) 1907999.

[82] Y. Zou, P. Tan, B. Shi, H. Ouyang, D. Jiang, Z. Liu, H. Li, M. Yu, C. Wang, X. Qu, L. Zhao, Y. Fan, Z.L. Wang, Z. Li, A bionic stretchable nanogenerator for underwater sensing and energy harvesting, Nat. Commun. 10 (2019) 2695.

[83] B. Shi, Z. Liu, Q. Zheng, J. Meng, H. Ouyang, Y. Zou, D. Jiang, X. Qu, M. Yu, L. Zhao, Y. Fan, Z.L. Wang, Z. Li, Body-integrated self-powered system for wearable and implantable applications, ACS Nano 13 (2019) 6017–6024.

[84] J. Sun, A. Yang, C. Zhao, F. Liu, Z. Li, Recent progress of nanogenerators acting as biomedical sensors in vivo, Sci. Bull. 64 (2019) 1336–1347.

[85] L. Zhao, H. Li, J. Meng, Z. Li, The recent advances in self-powered medical information sensors, InfoMat 2 (2020) 212–234.

[86] H. Liu, W. Dong, Y. Li, F. Li, J. Geng, M. Zhu, T. Chen, H. Zhang, L. Sun, C. Lee, An epidermal sEMG tattoo-like patch as a new human – machine interface for patients with loss of voice, Microsys Nanoeng. 6 (2020) 16.

[87] T. Chen, Q. Shi, M. Zhu, T. He, Z. Yang, H. Liu, L. Sun, L. Yang, C. Lee, Intuitive-augmented human-machine multidimensional nano-manipulation terminal using triboelectric stretchable strip sensors based on minimalist design, Nano Energy 60 (2019) 440–448.

[88] H. Liu, J. Zhong, C. Lee, S. Lee, L. Lin, A comprehensive review on piezoelectric energy harvesting technology: materials, mechanisms, and applications, Appl. Phys. Rev. 5 (2018), 041306.

[89] H. Liu, C. Hou, J. Lin, Y. Li, Q. Shi, T. Chen, L. Sun, C. Lee, A non-resonant rotational electromagnetic energy harvester for low-frequency and irregular human motion, Appl. Phys. Lett. 113 (2018) 203901.

[90] T. Chen, Q. Shi, K. Li, Z. Yang, H. Liu, L. Sun, J. Dziuban, C. Lee, Investigation of position sensing and energy harvesting of a triboelectric touch patch, Nanomaterials 8 (2018) 613.

Zhihao Ren received his B.Sc. degree from the School of Physics at the University of Electronic Science and Technology of China (UESTC), Chengdu, China, in 2017 After that he received his M. Sc. degree in Electrical and Computer Engineering (ECE) from National University of Singapore (NUS). He is currently a Research Engineer in the Department of ECE, NUS. His research interests are focused on mid-IR chemical sensors on meta-materials and nanophotonics for biomedical applications.

Dr. Jianxiong Zhu received his B.Eng. degree in Electrical and Automation Engineering from the Hubei University of Technology in 2006. After that, he got his Master's degree from the University of Science and Technology of China and Ph.D. from the University of Missouri Columbia in 2015. He is currently a Research Fellow of ECE, NUS. His research interests are focused on MEMS zero-power sensor, wearable flexible sensor, and gas sensor.

Dr. Qiongfeng Shi received his B.Eng. degree from the Department of Electronic Engineering and Information Science, University of Science and Technology of China (USTC) in 2012, and received his Ph.D. degree from the Department of Electrical and Computer Engineering, National University of Singapore (NUS) in 2018. He is currently a Research Fellow in the Department of Electrical and Computer Engineering, National University of Singapore. His research interests include energy harvesters, triboelectric nanogenerators, self-powered sensors, and wearable/implantable electronics.

Associate Prof. Hao Wang received his B.Eng. degree in School of Optoelectronic Information from University of Electronic Science and Technology of China in 2010, and Ph.D. degree from the National University of Singapore in 2016. He is currently a Research Associate of SIAT (Shenzhen Institutes of Advanced Technology), China. His research interests are focused on nanoneedle devices for transdermal drug delivery, flexible and wearable electronics, energy harvesting and electrical neural stimulations.

Weixin Liu received his B. Eng degree in Mechatronics Engineering from the School of Mechanical Engineering at Zhejiang University, Hangzhou, China, in 2019. He is currently a Research Assistant in the Dept. of ECE, NUS. His research interests focus mainly on MEMS piezoelectric resonant sensors and actuators.

Zixuan Zhang received his B.Eng. degree from the School of Mechanical and Electrical Engineering at the University of Electronic Science and Technology of China (UESTC), Chengdu, China, in 2018. He is now a Master student in the Department of Electrical and Computer Engineering, National University of Singapore. His research interests include self-powered wearable sensors, energy harvesters and triboelectric nanogenerators.

Prof. Chengkuo Lee received his Ph.D. degree in Precision Engineering from The University of Tokyo in 1996. Currently, he is the director of the Center for Intelligent Sensors and MEMS at the National University of Singapore, Singapore. He was a Senior Member of IEEE. He has contributed to more than 300 peer-reviewed international journal articles. His ORCID is 0000- 0002-8886-3649.